Biomineralization

DOI: 10.1002/ange.201210259

Multiphase Intrafibrillar Mineralization of Collagen**

Li-na Niu, Kai Jiao, Heonjune Ryou, Cynthia K. Y. Yiu, Ji-hua Chen, Lorenzo Breschi, Dwayne D. Arola, David H. Pashley, and Franklin R. Tay**

In the past, the two major biomineralization motifs, biosilicification and biocalcification, were considered as two discrete processes. However, there is increasing evidence of the existence of an inextricable relationship between biosilica and calcium-based biominerals.[1] The recent discovery of a unique silica–chitin–aragonite biocomposite in one genus of demosponges (*Verongida*) introduces a novel mechanism of multiphase hierarchical biomineralization.[2] Considerable effort has been devoted to the development of silica-/calcium-based organic–inorganic hybrids;[3–5] however, none of the techniques used could demonstrate the composite nature of their natural counterparts. Herein, we report a bottom-up, biomimetic biomineralization strategy that results in the intrafibrillar mineralization of collagen with hierarchically arranged silica–apatite multiphase minerals. The mineralization mechanism involves the precipitation and crystal growth of polymer-induced amorphous calcium phosphate precursors within the intrafibrillar spaces of hierarchically silicified collagen. Silicified-collagen-templated intrafibrillar apatite formation provides a model for the formation of multiphase-mineralized skeletons in invertebrates and also results in a biocomposite with increased fatigue resistance and resilience owing to the interpenetrating arrangement of amorphous silica, collagen, and crystalline apatite; the biocomposite also demonstrates enhanced bioactivity, biocompatibility, and potential for the correction of bone defects as a result of the presence of these multiphase components.[1,6,7]

Nature has destined each organism to receive one mineral (silica, calcium carbonate, or calcium phosphate) as their primary skeletal building block. Nevertheless, genuine multiphase mineralization does exist. Examples include silica–chitin–aragonite skeletons in Demosponges, opal–chitin–goethite radulae in molluscs, silica–chitin–apatite shells in Brachiopods, and silica–chitin–willenite teeth in Copepods.[1,2,8–10] These rare natural multiphase biominerals provide evolutionary insight into biomineralization and inspiration for the development of novel multiphase-mineralized biocomposites. A unique biocomposite from the order Verongida (*V. gigantea*) is a representative example of natural multiphase mineralization, with a three-dimensional matrix of silicified chitin fibrils infiltrated by regularly distributed aragonite crystals within the siliceous construct.[2] We previously reported a multiphase-mineralized eggshell membrane (ESM) created by introducing nanostructured calcium phosphate or silica into the different compartmental niches of the biopolymer membrane by the use of amorphous precursor phases of the corresponding mineral.[5] The differential distribution of calcium phosphate and silica in the ESM is attributed to the different organic composition of the fiber cores and mantles and represents a different phenomenon from the multiphase mineralization in Verongida, in which two different minerals are arranged hierarchically within one organic template. As the in vitro biomimetic intrafibrillar calcification and intrafibrillar silicification of type I collagen were both described recently,[11,12] we examined the possibility of the intrafibrillar hierarchical multiphase mineralization of type I collagen through a biomimetic strategy with the expectation that novel multiphase biocomposites could result.

In the present multiphase biomimetic mineralization strategy, poly(allylamine hydrochloride)-stabilized silicic acid (PAH–SA) and poly(aspartic acid)-stabilized amorphous calcium phosphate (PAsp–ACP) were used for the in vitro intrafibrillar silicification and calcification, respectively, of type I collagen through stepwise bottom-up approaches (see section S2 in the Supporting Information).[11,12] Collagen

[*] Dr. D. H. Pashley, Dr. F. R. Tay
School of Graduate Studies, Georgia Regents University
Augusta, GA 30912-1129 (USA)
E-mail: tayfranklin7@gmail.com
Dr. L. N. Niu, Dr. K. Jiao, Dr. J. H. Chen
School of Stomatology, Fourth Military Medical University
Xi'an (P.R. China)
E-mail: jhchen@fmmu.edu.cn
Dr. H. Ryou, Dr. D. D. Arola
Department of Mechanical Engineering
University of Maryland Baltimore County
Baltimore, Maryland, 21250 (USA)
Dr. C. K. Y. Yiu
Prince Philip Dental Hospital, The University of Hong Kong
Hong Kong SAR (P.R. China)
Dr. L. Breschi
Department of Medical Sciences, University of Trieste
Trieste; IGM, C.N.R.–IOR, Bologna (Italy)

[**] This research was supported by grant R01 DE015306-06 from NIDCR (to D.H.P.), ERA and IRRM awards from Georgia Health Sciences University (to F.R.T.), National Nature Science Foundation of China grant 81130078 (to J.H.C.), and National Key Basic Research Program of China grant 2012CB526704 (to J.H.C.). The murine mesenchymal stem cell line employed in this study was provided by the Texas A&M Health Science Center College of Medicine, Institute for Regenerative Medicine at Scott & White Hospital through grant P40-RR-017447 from the National Center for Research Resources, U.S. National Institutes of Health. We thank Frankie Chan from the University of Hong Kong for his help in STEM–EDX analysis.

Supporting information for this article is available on the WWW under http://dx.doi.org/10.1002/anie.201210259.

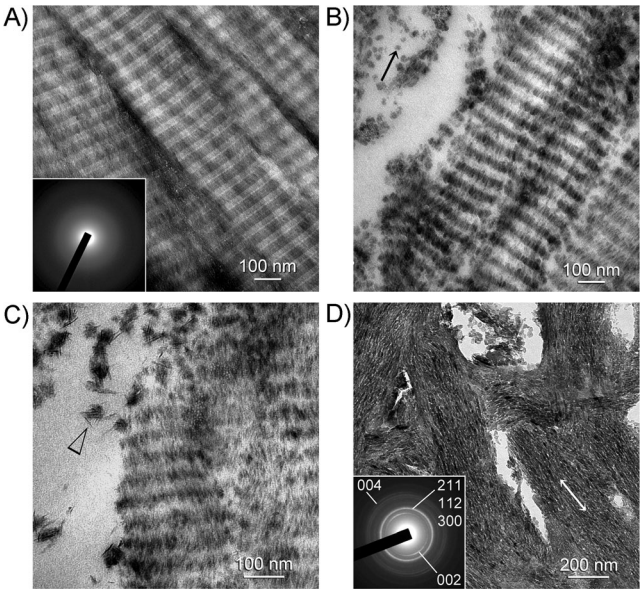

Figure 1. TEM images of unstained multiphase-mineralized collagen sponge. A) The collagen sponge was heavily silicified after incubation in PAH–SA for 2 days. Electron-dense intrafibrillar minerals replicate the cross-banding and microfibrillar architecture of fibrillar collagen. Inset: Selected-area electron diffraction reveals the amorphous nature of the infiltrated minerals. B) During the initial stage of multiphase mineralization (2 days), PAsp–ACP particles (arrow) infiltrated into the collagen fibril and nucleated along the preformed intrafibrillar silica. The band structure of the silicified collagen fibrils can still be clearly distinguished at this stage. C) During further incubation in a solution of PAsp–ACP (4 days), the transformation of ACP into nanometer-sized apatite crystallites could be identified (arrowhead). The elongated growth of the intrafibrillar apatite consumes more intrafibrillar space and gradually masks the banding structure of silicified collagen. D) After 7 days of incubation in a solution of PAsp–ACP solution, the apatite crystallites organized themselves along the longitudinal axis of the collagen fibrils and filled all the intrafibrillar spaces (double-headed arrow). The band structure of the silicified collagen cannot be distinguished. Inset: Selected-area electron diffraction indicates the crystalline nature of the newly formed minerals, with diffraction patterns that are characteristic of apatite.

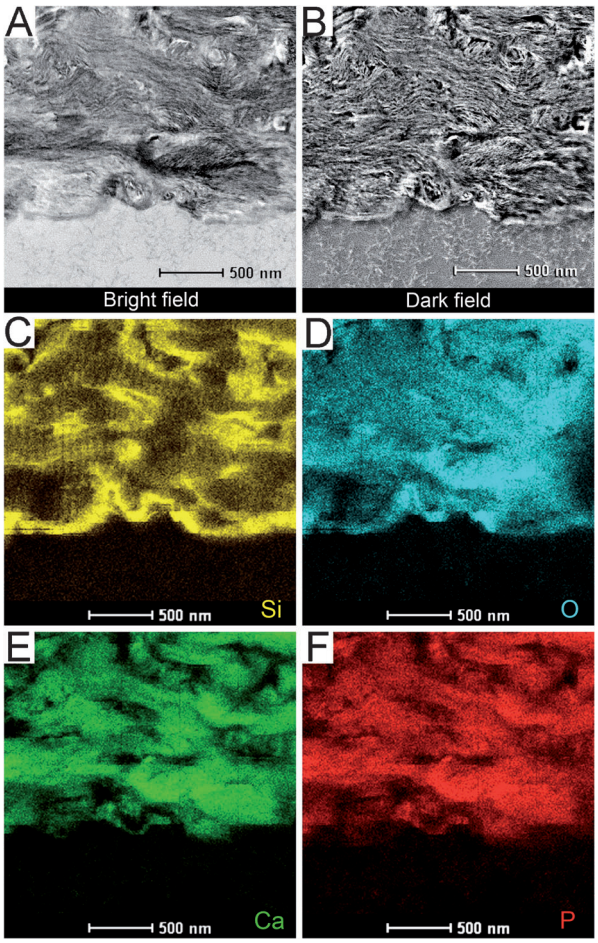

Figure 2. Elemental analysis (STEM–EDX) of a non-osmicated, unstained section of a collagen fiber confirms the multiphase nature of the mineralized collagen sponge. A,B) Bright- and dark-field images reveal the presence of electron-dense minerals deposited predominantly within the collagen fibrils. C–F) Elemental mapping indicates that silicon, oxygen, calcium, and phosphate are present simultaneously within the collagen fibrils. Silicon mapping shows regular collagen *D* spacings, which are attributed to the presence of intrafibrillar silicon. The manifestation of calcium and phosphorus signals inside the collagen fibrils is indicative of the coexistence of intrafibrillar calcification.

sponges were silicified with PAH–SA for 2 days and then incubated in PAsp–ACP for 7 days (Figure 1). During the second phase (intrafibrillar apatite deposition) of multiphase mineralization, apatite crystallites formed around the intrafibrillar silica by the fourth day, and both intrafibrillar platelike apatite and the band characteristics of silicified collagen could be distinguished (Figure 1 C). After 7 days, elongated electron-dense crystallites occupied the entire volume of the intrafibrillar spaces and thus masked the band characteristics of silicified collagen. Scanning transmission electron microscopy–energy-dispersive X-ray analysis (STEM–EDX) revealed the multiphase nature of the mineralized collagen scaffold, as indicated by the silicon-band structure caused by the selective condensation of silica inside the collagen fibril, and the intrafibrillar deposition of calcium phosphate based minerals (Figure 2). A three-dimensional matrix similar to the multiphase skeleton of Verongida was produced, whereby apatite crystallites were distributed intrafibrillarly within the siliceous collagen matrix. In the absence of PAsp as a stabilization agent for calcium phosphate, large crystals were formed only on the surface of the silicified collagen fibrils (see section S3 in the Supporting Information).

Attenuated total reflection Fourier transform infrared spectroscopy of the multiphase-mineralized collagen scaffold (see Figure S4 in the Supporting Information) revealed both the Si–O–Si vibrational modes of silica (TO_3, TO_2, and TO_1) and the O–P–O bending modes of apatite (υ_3PO_4, υ_4PO_4, υ_2PO_4, and υ_1PO_4).[5,11] The υ_3C–O stretching mode at 1413 cm^{-1} is indicative of carbonate substitution of the apatite lattice.[5] Inorganic phases within the multiphase-mineralized collagen scaffold were identified by $^1H \rightarrow {}^{29}Si$ cross-polarization magic angle spinning (CP MAS) solid-state nuclear magnetic resonance spectroscopy and ^{31}P MAS NMR spectroscopy (Figure 3). The broad peak between −100 and

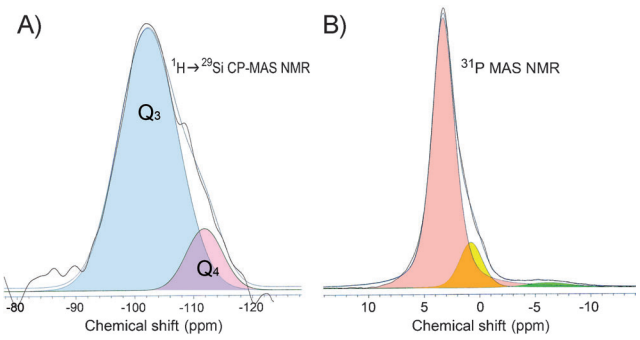

Figure 3. Solid-state NMR spectra of multiphase-mineralized collagen sponge. A) $^{1}H \rightarrow ^{29}Si$ CP MAS NMR spectrum. The two signals at −100 and −110 ppm correspond to Q_3 ($Si(OSi)_3(OH)$) and Q_4 (SiO_4). No Q_1 ($SiO(OH)_3$) and Q_2 ($SiO_2(OH)_2$) signals at −88 and −91 ppm were identified. B) ^{31}P MAS NMR spectrum. The three ^{31}P resonances identified at 3.2, 0.78, and −6.17 ppm correspond to PO_4^{3-}, HPO_4^{2-}, and P–O–Si moieties, respectively.

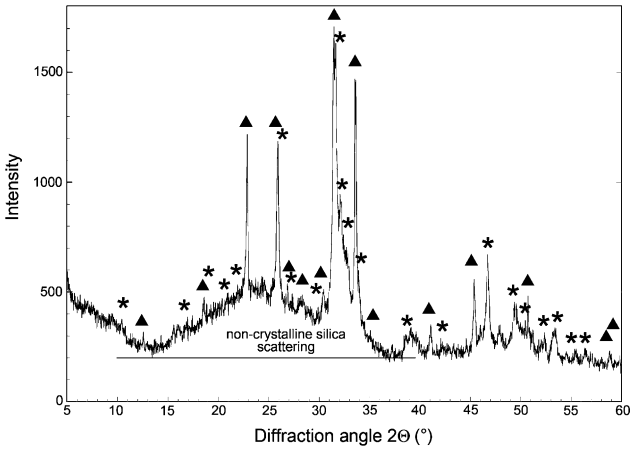

Figure 4. X-ray diffraction spectrum of multiphase-mineralized collagen sponge. The broad background peak is due to amorphous silica. The crystalline parts of the hybrid material were assigned as hydroxyapatite, $Ca_5(PO_4)_3(OH)$ (star, JCPD #09-0432) and nagelschmidtite, $Ca_7(SiO_4)_2(PO_4)_2$ (triangle, JCPD #11-0676).

−125 ppm in the $^{1}H \rightarrow ^{29}Si$ CP MAS NMR spectrum was deconvoluted to reveal the Q_3 ($Si(OSi)_3(OH)$) and Q_4 (SiO_4) peaks at −100 and −110 ppm, respectively,[13] which are indicative of the condensation of a hydrated silica phase within the biocomposite. The ^{31}P MAS NMR spectrum revealed three ^{31}P resonances corresponding to PO_4^{3-}, HPO_4^{2-}, and P–O–Si at 3.2, 0.78, and −6.17 ppm, respectively, with an intensity ratio of 100:17.07:3.43.[13–15] The presence of a minute amount of a P–O–Si moiety indicates a reaction between the silanol group in the silicified collagen and HPO_4^{2-} or PO_4^{3-} ions.[15–17]

Powder X-ray diffraction of the multiphase-mineralized collagen scaffold (Figure 4) revealed a broad background spectrum from 13 to 37° that may be attributed to amorphous silica. Distinct fractions of hydroxyapatite ($Ca_5(PO_4)_3(OH)$) (JCPD# 09-0432) were identified.[18] The spectrum also shows diffraction corresponding to nagelschmidtite ($Ca_7(SiO_4)_2(PO_4)_2$) (JCPD# 11-0676), which is not normally formed under physiological conditions.[19] Thermogravimetric analysis revealed a mineral content of 78.7 wt % in the multiphase-mineralized collagen scaffold (see Figure S5 in the Supporting Information). The derivative weight-loss curve indicated three major episodes at 20–200, 300–500, and 700–900 °C. The first weight loss corresponds to the elimination of physisorbed water as reflected by the peaks at 41.3, 121.3, and 189.0 °C. The second weight loss is reflected by peaks centered around 350.2 and 486.9 °C, which are due to the decomposition of collagen molecules. The third weight loss from 772.7–830.2 °C is attributed to combustion of the organic matrix and the release of CO_2 from carbonated apatite.[20]

To further delineate the spatial relationship between amorphous silica and crystalline apatite within the collagen fibril, we dissolved the multiphase biocomposite selectively in an acidic or an alkaline solution to remove apatite or silica, respectively (see Figure S6 in the Supporting Information). Our results confirmed the coexistence of siliceous and apatitic intrafibrillar phases within the collagen fibril. The synthesis of the silica–collagen–apatite biocomposite in the present study is analogous to the proposed mechanism for multiphase mineralization in the silica–chitin–aragonite biocomposite of *V. gigantean*[2] and can be viewed as a novel nanotechnology involving the organization of apatite crystallites in the presence of polymeric silica, which provides niduses for apatite growth. As the PAH-stabilized, "soluble" silicic acid precursors infiltrate the collagen fibrils, they condense at specific sites along the collagen triple helix.[11,21] The hierarchically silicified collagen fibrils containing multiple negative silanol groups sequestrate calcium from fluidic PAsp-stabilized ACPs that are small enough to infiltrate the silicified collagen. In this way, calcium phosphate phases are deposited over the original amorphous silica phase.[12,22] During the later stages of biocalcification, crystalline apatite phases fill the entire intrafibrillar spaces of the amorphous silicified collagen fibril and thus mask the original silica phase.[23]

The multiphase biomineralization strategy was further confirmed by the use of rat-tail-tendon collagen as a naturally occurring soft-tissue model substrate (see Figure S7 in the Supporting Information). Because of the coexistence of different intrafibrillar minerals, changes in the mechanical properties of the biocomposites are to be expected. Thus, nanoscopic dynamic mechanical analysis was used to investigate the effect of biosilicification, biocalcification, and multiphase mineralization on the biomechanical properties of rat-tail collagen by the indentation and analysis of hydrated samples with a triboindenter system. The complex modulus (total elastic and dampening capacity of a material), storage modulus (elastic response of a material), and loss modulus (viscous response of a material) of silicified rat-tail collagen were significantly lower than the corresponding values for multiphase-mineralized rat-tail collagen and calcified rat-tail collagen ($P < 0.05$; Figure 5), since the modulus of elasticity of amorphous siliceous minerals is lower than that of crystalline mineral phases. Tan δ values (ability of a material to absorb energy) derived for the three types of mineralized rat-tail collagen revealed significant differences in their

damping capacity, in the order: silicified collagen > multiphase-mineralized collagen > calcified collagen ($P < 0.05$). This stepwise decrease in the dampening capacity is a reflection of the increase in the crystalline mineral phase and the decrease in the amorphous mineral phase within these collagen matrices, whereby the multiphase-mineralized biocomposites exhibit a balance between the properties of stiffness and resilience. These nanoscopic mechanical properties found for rat-tail collagen were further confirmed by analysis of the compressive stress–strain response (tangent modulus and modulus of toughness) in macroscopic specimens of hydrated biosilicified, biocalcified, and multiphase-mineralized collagen sponges (see Figure S8 in the Supporting Information).

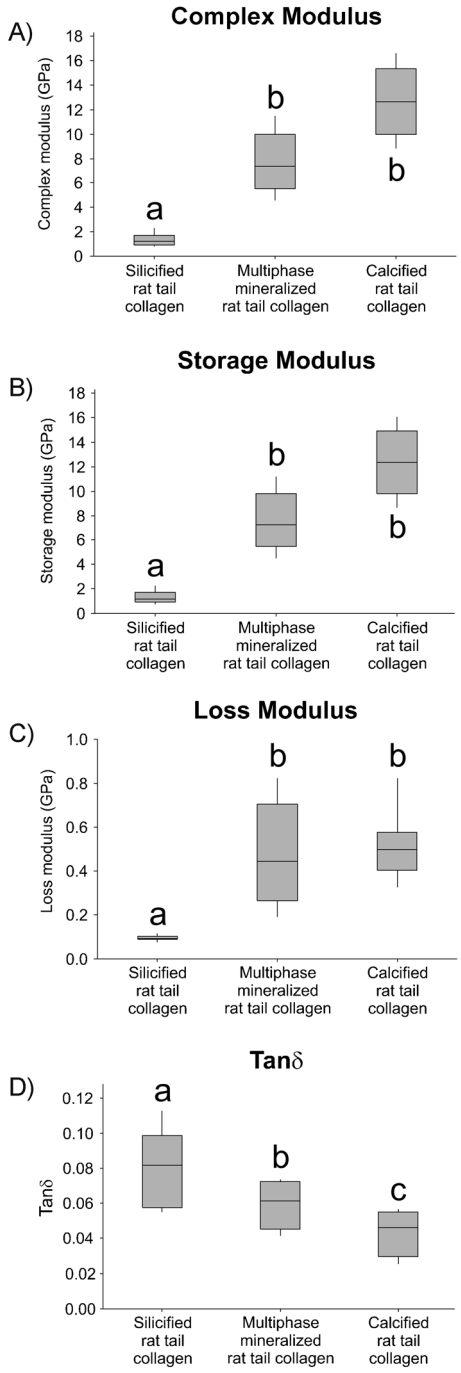

Figure 5. Box plots summarizing the nanoscopic dynamic mechanical properties of silicified, calcified, and multiphase-mineralized rat-tail collagen: A) complex modulus; B) storage modulus; C) loss modulus; D) tan δ. Each box plot shows the minimum value, 25th percentile, median, 75th percentile, and maximum value of a data set ($N = 10$). For each parameter, groups designated by the same letter are not statistically different (one-way ANOVA and Holm–Sidak post-hoc multiple comparisons; $P > 0.05$).

In the silica–chitin–aragonite biocomposite of *V. giganteam*, a chitinous template is used for deposition of aragonite crystalline aggregates over silicified chitin.[2] Because type I collagen is widely distributed in both invertebrates and vertebrates and possesses high tensile strength, low antigenicity, and controllable biodegradation properties, it was chosen as the template for biomimetic multiphase mineralization in the present study.[1,23] Silica and carbonated apatite were chosen as the mineral components in our multiphase-mineralization model because of their wide distribution in the biological world. The resulting silica–collagen–apatite biocomposite indicates that two separate minerals, one in an amorphous form and the other in crystalline form, may be introduced simultaneously into the intrafibrillar spaces between tropocollagen molecules.

The viability of the multiphase mineralization strategy was further confirmed by the use of demineralized bovine trabecular bone matrix as a naturally occurring hard-tissue model substrate. Microcomputed tomography showed the homogeneous mineralization of multiphase-mineralized bone specimens (see Figure S9 in the Supporting Information). It is speculated that the novel biomaterial will combine the biocompatibility and osteoinductivity of a demineralized bone matrix,[24] the ability of silica to promote collagen synthesis and neovascularization,[25] and the osteoconductive and integrative properties of calcium phosphate minerals.[26] The biocompatibility of the remineralized specimens was investigated with a mouse mesenchymal stem cell line (mMSC) expressing the green fluorescent protein. The results demonstrate that multiphase-mineralized bovine trabecular bone scaffolds are highly biocompatible and suitable for the adhesion of mMSCs and their infiltration into the scaffolds (see section S10 in the Supporting Information). Further studies need to be performed to examine the osteoinductivity of these novel scaffolds.

The current multiphase-mineralization process also contributes to our understanding of the effect of silicon on bone formation, a phenomenon that has been studied since the 1970s. Carlisle as well as Schwarz and Milne showed that silicon is present in active calcification sites in young mouse and rat bone. In animal trials, silicon deficiency results in abnormal bone formation with decreased deposition of both the extracellular matrix and bone mineral (apatite).[6,7] A positive association between dietary silicon intake and bone-mineral density was also found in a human study.[27] It is generally thought that silicon stimulates human osteoblasts and osteoblast-like cells to secrete type I collagen and other biochemical markers of osteoblast maturation and bone formation.[28] Although bone formation and metabolism are mainly controlled by different types of cells in a living

organism, the presence of silica along the calcification front may enhance the role of collagen as a template for intrafibrillar apatite deposition, as the polysilanol groups of the amorphous silica could serve as niduses for apatite growth. Thus, we speculate that a similar multiphase silica–collagen–apatite structure may exist during the initial process of natural bone formation. Differences in the mechanical properties of silicified collagen, multiphase-mineralized collagen, and calcified collagen may help explain a phenomenon that occurs with aging: mature bone tissue contains a higher apatite concentration (i.e. is more brittle) and a lower silicon concentration (i.e. shows decreased resilience) than newly formed bone. This difference may account for the increasing risk of bone fracture with aging.[29]

In summary, we have described a novel multiphase intrafibrillar mineralization scheme that is important for understanding the diversity of biomineralization. Further studies will focus on the biological application of this biocomposite in hard-tissue regeneration.

Received: December 24, 2012
Published online: April 18, 2013

Keywords: biomineralization · calcification · crystal growth · fibrous proteins · silicification

[1] H. Ehrlich in *Biologically-Inspired Systems*, *Vol. 1* (Eds.: S. N. Gorb), Springer, Dordrecht, **2010**, pp. 51 – 91.
[2] H. Ehrlich, et al., *Chem. Mater.* **2010**, *22*, 1462 – 1471 (see the Supporting Information, section S11, reference S3).
[3] S. Heinemann, C. Heinemann, R. Bernhardt, A. Reinstorf, B. Nies, M. Meyer, H. Worch, T. Hanke, *Acta Biomater.* **2009**, *5*, 1979 – 1990.
[4] S. Hesaraki, M. Alizadeh, S. Borhan, M. Pourbaghi-Masouleh, *J. Biomed. Mater. Res. Part B* **2012**, *100*, 1627 – 1635.
[5] N. Li, L. N. Niu, Y. P. Qi, C. K. Yiu, H. Ryou, D. D. Arola, J. H. Chen, D. H. Pashley, F. R. Tay, *Biomaterials* **2011**, *32*, 8743 – 8752.
[6] E. M. Carlisle, *Science* **1972**, *178*, 279 – 280.
[7] K. Schwarz, D. B. Milne, *Nature* **1972**, *239*, 333 – 334.
[8] T. E. Hua, C. W. Li, *Zool. Stud.* **2007**, *46*, 379 – 388.
[9] C. Lüter, *Proc. R. Soc. London Ser. B* **2004**, *271*, 465 – 467.
[10] C. B. Miller, D. M. Nelson, C. Weiss, A. H. Soeldner, *Mar. Biol.* **1990**, *106*, 91 – 101.
[11] L. N. Niu, K. Jiao, Y. P. Qi, C. K. Yiu, H. Ryou, D. D. Arola, J. H. Chen, L. Breschi, D. H. Pashley, F. R. Tay, *Angew. Chem.* **2011**, *123*, 11892 – 11895; *Angew. Chem.* **2011**, *123*, 11892 – 11895; *Angew. Chem. Int. Ed.* **2011**, *50*, 11688 – 11691.
[12] T. T. Thula, F. Svedlund, D. E. Rodriguez, J. Podschun, L. Pendi, L. B. Gower, *Polymers* **2011**, *3*, 10 – 35.
[13] C. Gröger, K. Lutz, E. Brunner, *Prog. Nucl. Magn. Reson. Spectrosc.* **2009**, *54*, 54 – 68.
[14] J. Kolmas, A. Slósarczyk, A. Wojtowicz, W. Kolodziejski, *Solid State Nucl. Magn. Reson.* **2007**, *32*, 53 – 58.
[15] R. Mathew, P. N. Gunawidjaja, I. Izquierdo-Barba, K. Jansson, A. García, D. Arcos, M. Vallet-Regí, M. Edén, *J. Phys. Chem. C* **2011**, *115*, 20572 – 20582.
[16] P. N. Gunawidjaja, A. Y. H. Lo, I. Izquierdo-Barba, A. García, D. Arcos, B. Stevensson, J. Grins, M. Vallet-Regí, M. Edén, *J. Phys. Chem. C* **2010**, *114*, 19345 – 19356.
[17] E. Leonova, I. Izquierdo-Barba, D. Arcos, A. López-Noriega, N. Hedin, M. Vallet-Regí, M. Edén, *J. Phys. Chem. C* **2008**, *112*, 5552 – 5562.
[18] Y. K. Kim, L. S. Gu, T. E. Bryan, J. R. Kim, L. Chen, Y. Liu, J. C. Yoon, L. Breschi, D. H. Pashley, F. R. Tay, *Biomaterials* **2010**, *31*, 6618 – 6627.
[19] Y. Zhou, C. Wu, Y. Xiao, *Acta Biomater.* **2012**, *8*, 2307 – 2316.
[20] A. Sola, D. Bellucci, M. G. Raucci, S. Zeppetelli, L. Ambrosio, V. Cannillo, *J. Eur. Ceram. Soc.* **2006**, *26*, 537 – 542.
[21] M. Sumper, *Angew. Chem.* **2004**, *116*, 2301 – 2304; *Angew. Chem. Int. Ed.* **2004**, *43*, 2251 – 2254.
[22] N. Sahai, M. Anseau, *Biomaterials* **2005**, *26*, 5763 – 5770.
[23] F. Nudelman, K. Pieterse, A. George, P. H. Bomans, H. Friedrich, L. J. Brylka, P. A. Hilbers, G. de With, N. A. Sommerdijk, *Nat. Mater.* **2010**, *9*, 1004 – 1009.
[24] N. M. Coseo, N. Saldua, J. Harrop, *J. Neurosurg. Sci.* **2012**, *56*, 203 – 207.
[25] L. N. Niu, et al., *FASEB J.* **2012**, *26*, 4517 – 4529 (see the Supporting Information, section S11, reference S13).
[26] D. J. Hak, *J. Am. Acad. Orthop. Surg.* **2007**, *15*, 525 – 536.
[27] R. Jugdaohsingh, K. L. Tucker, N. Qiao, L. A. Cupples, D. P. Kiel, J. J. Powell, *J. Bone Miner. Res.* **2004**, *19*, 297 – 307.
[28] W. Waked, J. Grauer, *Orthopedics* **2008**, *31*, 591 – 597.
[29] K. S. Chan, C. K. Chan, D. P. Nicolella, *Bone* **2009**, *45*, 427 – 434.

